Conference or Workshop Item:
Alosaimi, M and Lesnic, D (Accepted: 2023) Solution of a physical problem in bioheat transfer via a meshless approach. In: 13th UK Conference on Boundary Integral Methods (UKBIM13), 10-11 Jul 2023, Aberdeen, UK. (Unpublished)

Chapter 1

Solution of a physical problem in bioheat transfer via a meshless approach

M. Alosaimi[1] and D. Lesnic[2]

[1] Department of Mathematics and Statistics,
Taif University
College of Science, P.O. Box 11099, Taif 21944, Saudi Arabia
m.alosaimi@tu.edu.sa

[2] Department of Applied Mathematics,
University of Leeds
Leeds LS2 9JT, UK
D.Lesnic@leeds.ac.uk

Abstract. *The physical direct problem of determining the temperature distribution in a single-layer two-dimensional biological skin tissue is considered. This problem arises in hyperthermia applications where one aims to obtain knowledge of temperature distribution through a biological tissue that is subjected to instantaneous heating. Due to the finite speed of heat propagation, the appropriate mathematical model is described by a hyperbolic thermal-wave model of bio-heat transfer. Such a model is numerically solved using the time-marching method of fundamental solutions, as well as an alternating direction implicit scheme. The results obtained by the two numerical methods are discussed and compared, and excellent agreement is achieved.*

1.1 Introduction

One model that takes into account the transient mechanisms of heat transfer in biological tissues is based on the Pennes' parabolic reaction-diffusion equation (obtained by taking $\tau = 0$ in equation (1.1) below), which was proposed to model the temperature evolution during cancer hyperthermia treatment [12], the thermal radiation from cellular phones [13] and the ablation of afflicted tissues [4], among others. However, although still widely used, the Pennes parabolic model of heat transfer implies infinite speed of thermal propagation. This contradicts the physical reality that biological bodies, along with a number of other common materials, exhibit

a relatively long thermal relaxation (or lag) time τ (typically between 15 to 30 seconds), [9]. This contradiction is resolved by the thermal-wave model of bio-heat transfer given by the Maxwell-Cattaneo hyperbolic equation (1.1) defined in Section 1.2. Related to this equation, in this paper, we solve a direct physical problem of determining the temperature distribution in a single-layer, two-dimensional biological skin tissue by the time-marching method of fundamental solutions (TMMFS), as well as the alternating direction implicit (ADI) scheme. The results obtained by the two numerical methods are discussed and compared.

The paper is organized as follows. The mathematical formulation of the direct problem is presented in Section 1.2, and a non-dimensional form of it is derived. In Sections 1.3 and 1.4, the ADI scheme and the TMMFS are described. In Section 1.5, the numerical methods are implemented for the numerical solution of the model under consideration for a physical example concerning the determination of the temperature distribution in a biological tissue undergoing laser irradiation. Finally, Section 1.6 highlights the conclusions of the work.

1.2 Mathematical formulation

Let $\Omega = (0, \bar{L}_1) \times (0, \bar{L}_2)$ denote the spatial domain of a single-layer, two-dimensional biological skin tissue, where $\bar{L}_1 > 0$ and $\bar{L}_2 > 0$ stand for the depth and width of the tissue, respectively. The heat propagation in such a biological body is governed by the thermal-wave model of bio-heat transfer [8]

$$\rho_{\rm t} c_{\rm t} \tau \frac{\partial^2 T}{\partial \bar{t}^2} + (\rho_{\rm t} c_{\rm t} + \tau \rho_b c_b w_b) \frac{\partial T}{\partial \bar{t}} = \kappa \nabla^2 T + \rho_b c_b w_b (T_b - T) + Q_m + Q_e + \tau \frac{\partial}{\partial \bar{t}} (Q_m + Q_e), \quad (\bar{x}_1, \bar{x}_2, \bar{t}) \in \Omega \times (0, t_{\rm f}], \tag{1.1}$$

where T, $\rho_{\rm t}$, $c_{\rm t}$ and κ represent the temperature [°C], density [kg/m^3], specific heat [J/(kg °C)] and thermal conductivity [W/(m °C)] of the tissue, respectively, ρ_b, c_b and w_b stand for the density [kg/m^3], specific heat [J/(kg °C)] and perfusion rate [s^{-1}] of the blood, respectively, τ is the relaxation time [s] required for the thermal waves to propagate, T_b is the (arterial) blood temperature [°C], Q_m and Q_e are heat generations [W/m^3] due to metabolism and external heating, respectively, and $t_{\rm f}$ is the duration of the thermal process [s].

Consider equation (1.1) subject to the initial conditions

$$T(\bar{x}_1, \bar{x}_2, 0) = T_0(\bar{x}_1, \bar{x}_2), \quad \frac{\partial T}{\partial \bar{t}}(\bar{x}_1, \bar{x}_2, 0) = V_0(\bar{x}_1, \bar{x}_2), \quad (\bar{x}_1, \bar{x}_2) \in \Omega, \tag{1.2}$$

where T_0 and V_0 are prescribed functions, and the Dirichlet boundary condition

$$T(\bar{x}_1, \bar{x}_2, \bar{t}) = \mu(\bar{x}_1, \bar{x}_2, \bar{t}), \quad (\bar{x}_1, \bar{x}_2, \bar{t}) \in \partial\Omega \times [0, t_{\rm f}], \tag{1.3}$$

where μ is a prescribed function, assuming also the compatibility $\mu|_{\partial\Omega \times \{0\}} = T_0|_{\partial\Omega}$. Adiabatic or Robin boundary conditions can also be considered in place of the Dirichlet boundary condition (1.3). The hyperbolic model (1.1)–(1.3) can be non-dimensionalized, as follows:

$$(x_i, L_i) = \sqrt{\frac{\tau C_{\rm t}}{\kappa t_{\rm f}^2}} (\bar{x}_i, \bar{L}_i) \text{ for } i = 1, 2, \quad t = \frac{\bar{t}}{t_{\rm f}}, \quad u = \frac{T - T_b}{T_b}, \quad \phi = \frac{T_0 - T_b}{T_b}, \quad \psi = \frac{t_{\rm f} V_0}{T_b}, \quad \nu = \frac{\mu - T_b}{T_b}, \tag{1.4}$$

where the blood temperature T_b has been assumed uniform and equal to a non-zero constant.

Introducing the non-dimensional variables (1.4) into the thermal-wave model of bio-heat transfer (1.1)–(1.3) yields the dimensionless model:

$$\begin{cases} u_{tt} + a_1 u_t = u_{x_1x_1} + u_{x_2x_2} - a_2 u + g(x_1, x_2, t), & \mathbf{x} = (x_1, x_2) \in D,\ t \in (0, 1], \\ u(x_1, x_2, 0) = \phi(x_1, x_2), \quad u_t(x_1, x_2, 0) = \psi(x_1, x_2), & (x_1, x_2) \in D, \\ u(x_1, x_2, t) = \nu(x_1, x_2, t), & (x_1, x_2, t) \in \partial D \times [0, 1], \end{cases} \tag{1.5}$$

where $D = (0, L_1) \times (0, L_2)$ and

$$a_1 = \frac{t_{\mathrm{f}}}{\tau} + \frac{w_b C_b t_{\mathrm{f}}}{C_{\mathrm{t}}}, \quad a_2 = \frac{w_b C_b t_{\mathrm{f}}^2}{\tau C_{\mathrm{t}}}, \quad g(x_1, x_2, t) = \frac{t_{\mathrm{f}}^2}{\tau T_b C_{\mathrm{t}}} \left[Q_e + Q_m + \frac{\tau}{t_{\mathrm{f}}} \frac{\partial}{\partial t} (Q_e + Q_m) \right]. \tag{1.6}$$

The next two sections describe the two numerical methods for the solution of the direct initial-boundary value problem (1.5).

1.3 The alternating direction implicit (ADI) scheme

In this section, we describe the ADI scheme from [1, 11] for the numerical solution of the problem (1.5), as follows. Introducing the intermediate variable v as

$$v := u_t + a_1 u, \tag{1.7}$$

then the first equation in (1.5) can be rewritten as

$$v_t = u_{x_1x_1} + u_{x_2x_2} - a_2 u + g(x_1, x_2, t). \tag{1.8}$$

We subdivide the solution domain $\overline{D} \times [0, 1]$ into $M^{(1)}$, $M^{(2)}$ and N subintervals of equal step lengths $\Delta x_1 = L_1/M^{(1)}$, $\Delta x_2 = L_2/M^{(2)}$ and $\Delta t = 1/N$, respectively. At the node (x_{1i}, x_{2j}, t_n), we denote $u_{i,j}^n := u(x_{1i}, x_{2j}, t_n)$, $v_{i,j}^n := v(x_{1i}, x_{2j}, t_n)$ and $g_{i,j}^n := g(x_{1i}, x_{2j}, t_n)$, where $x_{1i} = i\Delta x_1$, $x_{2j} = j\Delta x_2$ and $t_n = n\Delta t$ for $i = \overline{0, M^{(1)}}$, $j = \overline{0, M^{(2)}}$ and $n = \overline{0, N}$.

The Crank–Nicolson method, which is unconditionally stable and second-order accurate in space and time, discretises (1.7) and (1.8) as:

$$\begin{aligned} \frac{u_{i,j}^{n+1} - u_{i,j}^n}{\Delta t} &= \frac{1}{2} \left(v_{i,j}^n - a_1 u_{i,j}^n + v_{i,j}^{n+1} - a_1 u_{i,j}^{n+1} \right), \\ & i = \overline{1, (M^{(1)} - 1)},\ j = \overline{1, (M^{(2)} - 1)},\ n = \overline{0, (N - 1)}, \end{aligned} \tag{1.9}$$

$$\begin{aligned} \frac{v_{i,j}^{n+1} - v_{i,j}^n}{\Delta t} &= \frac{1}{2} \left[\left(\frac{1}{(\Delta x_1)^2} \delta_{x_1}^2 + \frac{1}{(\Delta x_2)^2} \delta_{x_2}^2 - a_2 \right) \left(u_{i,j}^n + u_{i,j}^{n+1} \right) + g_{i,j}^n + g_{i,j}^{n+1} \right], \\ & i = \overline{1, (M^{(1)} - 1)},\ j = \overline{1, (M^{(2)} - 1)},\ n = \overline{0, (N - 1)}, \end{aligned} \tag{1.10}$$

where $\delta_{x_1}^2 u_{i,j}^n := u_{i-1,j}^n - 2u_{i,j}^n + u_{i+1,j}^n$ and $\delta_{x_2}^2 u_{i,j}^n := u_{i,j-1}^n - 2u_{i,j}^n + u_{i,j+1}^n$. Solving (1.9) for $v_{i,j}^{n+1}$, we obtain:

$$v_{i,j}^{n+1} = \left(a_1 + \frac{2}{\Delta t} \right) u_{i,j}^{n+1} + \left(a_1 - \frac{2}{\Delta t} \right) u_{i,j}^n - v_{i,j}^n, \tag{1.11}$$

for $i=\overline{1,(M^{(1)}-1)}$, $j=\overline{1,(M^{(2)}-1)}$ and $n=\overline{0,(N-1)}$. Introducing (1.11) into (1.10), we obtain:

$$\left(a_1+\frac{2}{\Delta t}\right)u_{i,j}^{n+1}+\left(a_1-\frac{2}{\Delta t}\right)u_{i,j}^{n}$$
$$=\frac{\Delta t}{2}\left(\frac{1}{(\Delta x_1)^2}\delta_{x_1}^2+\frac{1}{(\Delta x_2)^2}\delta_{x_2}^2-a_2\right)\left(u_{i,j}^{n}+u_{i,j}^{n+1}\right)+2v_{i,j}^{n}+\frac{\Delta t}{2}\left(g_{i,j}^{n}+g_{i,j}^{n+1}\right), \quad (1.12)$$

for $i=\overline{1,(M^{(1)}-1)}$, $j=\overline{1,(M^{(2)}-1)}$ and $n=\overline{0,(N-1)}$. Denoting $A:=a_1+\frac{2}{\Delta t}+\frac{a_2\Delta t}{2}$, equation (1.12) can be reorganized as:

$$\left[1-\frac{\Delta t}{2A}\left(\frac{1}{(\Delta x_1)^2}\delta_{x_1}^2+\frac{1}{(\Delta x_2)^2}\delta_{x_2}^2\right)\right]u_{i,j}^{n+1}=\left[1+\frac{\Delta t}{2A}\left(\frac{1}{(\Delta x_1)^2}\delta_{x_1}^2+\frac{1}{(\Delta x_2)^2}\delta_{x_2}^2\right)\right]u_{i,j}^{n}$$
$$+\frac{2}{A}\left[v_{i,j}^{n}-\left(a_1+\frac{a_4\Delta t}{2}\right)u_{i,j}^{n}\right]+\frac{\Delta t}{2A}\left(g_{i,j}^{n}+g_{i,j}^{n+1}\right), \quad (1.13)$$

for $i=\overline{1,(M^{(1)}-1)}$,$j=\overline{1,(M^{(2)}-1)}$ and $n=\overline{0,(N-1)}$.

The above finite-difference scheme is second-order accurate [1], and thus we can add to it any term of the same or higher order without affecting its order of accuracy. Since the term

$$\frac{(\Delta t)^2}{4A^2(\Delta x_1)^2(\Delta x_2)^2}\delta_{x_1}^2\delta_{x_2}^2\left(u_{i,j}^{n+1}-u_{i,j}^{n}\right)$$

is of higher order than the scheme's order of accuracy, it can be added to the left-hand side of (1.13) without altering its order. We then obtain

$$\left(1-\frac{\Delta t}{2A(\Delta x_1)^2}\delta_{x_1}^2\right)\left(1-\frac{\Delta t}{2A(\Delta x_2)^2}\delta_{x_2}^2\right)u_{i,j}^{n+1}$$
$$=\left(1+\frac{\Delta t}{2A(\Delta x_1)^2}\delta_{x_1}^2\right)\left(1+\frac{\Delta t}{2A(\Delta x_2)^2}\delta_{x_2}^2\right)u_{i,j}^{n}$$
$$+\frac{2}{A}\left[v_{i,j}^{n}-\left(a_1+\frac{a_2\Delta t}{2}\right)u_{i,j}^{n}\right]+\frac{\Delta t}{2A}\left(g_{i,j}^{n}+g_{i,j}^{n+1}\right), \quad (1.14)$$

for $i=\overline{1,(M^{(1)}-1)}$, $j=\overline{1,(M^{(2)}-1)}$ and $n=\overline{0,(N-1)}$. Introducing an intermediate variable $u_{i,j}^{n+\frac{1}{2}}$, see [1, 11], we obtain the Peaceman-Rachford (PR)-like splitting scheme

$$\left(1-\frac{\Delta t}{2A(\Delta x_1)^2}\delta_{x_1}^2\right)u_{i,j}^{n+\frac{1}{2}}=\left(1+\frac{\Delta t}{2A(\Delta x_2)^2}\delta_{x_2}^2\right)u_{i,j}^{n}$$
$$+\frac{1}{A}\left[v_{i,j}^{n}-\left(a_1+\frac{a_2\Delta t}{2}\right)u_{i,j}^{n}\right]+\frac{\Delta t}{4A}\left(g_{i,j}^{n}+g_{i,j}^{n+1}\right), \quad (1.15)$$
$$\left(1-\frac{\Delta t}{2A(\Delta x_2)^2}\delta_{x_2}^2\right)u_{i,j}^{n+1}=\left(1+\frac{\Delta t}{2A(\Delta x_1)^2}\delta_{x_1}^2\right)u_{i,j}^{n+\frac{1}{2}}$$
$$+\frac{1}{A}\left[v_{i,j}^{n}-\left(a_1+\frac{a_2\Delta t}{2}\right)u_{i,j}^{n}\right]+\frac{\Delta t}{4A}\left(g_{i,j}^{n}+g_{i,j}^{n+1}\right), \quad (1.16)$$
$$v_{i,j}^{n+1}=\left(a_1+\frac{2}{\Delta t}\right)u_{i,j}^{n+1}+\left(a_1-\frac{2}{\Delta t}\right)u_{i,j}^{n}-v_{i,j}^{n}, \quad (1.17)$$

for $i = \overline{1,(M^{(1)}-1)}$, $j = \overline{1,(M^{(2)}-1)}$ and $n = \overline{0,(N-1)}$. In equations (1.15) and (1.16), the values of $u_{0,j}^{n+1}$ and $u_{M^{(1)},j}^{n+1}$ for $j = \overline{1,(M^{(2)}-1)}$ and $n = \overline{0,(N-1)}$ are needed. To obtain these values, we add equations (1.15) and (1.16) to get

$$u_{i,j}^{n+\frac{1}{2}} = \frac{u_{i,j}^{n+1} + u_{i,j}^{n}}{2} - \frac{\Delta t}{4A(\Delta x_2)^2}\delta_{x_2}^2\left(u_{i,j}^{n+1} - u_{i,j}^{n}\right), \tag{1.18}$$

although we usually use the simpler approximation [11],

$$u_{i,j}^{n+\frac{1}{2}} = \frac{u_{i,j}^{n+1} + u_{i,j}^{n}}{2}, \tag{1.19}$$

for $i = 0, M^{(1)}$, $j = \overline{1,(M^{(2)}-1)}$ and $n = \overline{0,(N-1)}$.

1.4 The time-marching method of fundamental solutions

In the TMMFS, one proceeds by first discretising the governing hyperbolic partial differential equation in (1.5) in time. The resulting Poisson-type equation is then solved by a combination of the method of fundamental solutions (MFS) and the method of particular solutions (MPS). For the time discretization, we select the Houbolt finite-difference scheme [3]. The first- and second-order time approximations are given by [3, 7]

$$\frac{\partial u^{n+1}}{\partial t} \approx \frac{1}{6h}\left(11u^{n+1} - 18u^{n} + 9u^{n-1} - 2u^{n-2}\right), \tag{1.20}$$

$$\frac{\partial^2 u^{n+1}}{\partial t^2} \approx \frac{1}{h^2}\left(2u^{n+1} - 5u^{n} + 4u^{n-1} - u^{n-2}\right), \tag{1.21}$$

where $u^n := u(\mathbf{x}, t^n)$, $t^n = nh$, $h > 0$ is the time step and n stands for the time level. Substituting (1.20) and (1.21) into the PDE equation in (1.5), we obtain

$$\nabla^2 u^{n+1} = C_0 u^{n+1} + C_1 u^{n} + C_2 u^{n-1} + C_3 u^{n-2} - g(\mathbf{x}, t^{n+1}), \tag{1.22}$$

where:

$$C_0 = \frac{2}{h^2} + \frac{11a_1}{6h} + a_2, \quad C_1 = -\frac{5}{h^2} - \frac{3a_1}{h}, \quad C_2 = \frac{4}{h^2} + \frac{3a_1}{2h}, \quad C_3 = -\frac{1}{h^2} - \frac{a_1}{3h}.$$

In the coupled MPS-MFS, the solution of the Poisson-type equation (1.22) can be written as

$$u^{n+1} = u_{\mathrm{P}}^{n+1} + u_{\mathrm{H}}^{n+1}, \tag{1.23}$$

where u_{P}^{n+1} is a particular solution that satisfies the non-homogeneous equation and u_{H}^{n+1} is the homogeneous solution satisfying the Laplace equation.

The particular solution u_{P}^{n+1} can be approximated by a linear combination of radial basis functions (RBFs), as follows:

$$u_{\mathrm{P}}^{n+1} = \sum_{j=1}^{n_{\mathrm{f}}} \beta_j^{n+1} F\left(\|\mathbf{x} - \mathbf{x}_j\|\right), \tag{1.24}$$

where $\left\{\beta_j^{n+1}\right\}_{j=\overline{1,n_\mathrm{f}}}$ are unknown coefficients to be determined by a collocation procedure and n_f is the number of the field points $\{\mathbf{x}_j\}_{j=\overline{1,n_\mathrm{f}}} \in D$. The function F can be obtained analytically by solving the Poisson equation

$$\nabla^2 F(r) = f(r), \tag{1.25}$$

where f is a radial basis function. Compactly supported radial basis functions (CSRBFs) are chosen to govern the particular solution [7], namely,

$$f(r) = \begin{cases} \left(1 - \frac{r}{\lambda}\right)^2, & r \le \lambda, \\ 0, & r > \lambda, \end{cases} \tag{1.26}$$

$$F(r) = \begin{cases} \frac{r^4}{16\lambda^2} - \frac{2r^3}{9\lambda} + \frac{r^2}{4}, & r \le \lambda, \\ \frac{13\lambda^2}{144} + \frac{\lambda^2}{12} \ln\left(\frac{r}{\lambda}\right), & r > \lambda, \end{cases} \tag{1.27}$$

where r is the distance between the field points and λ is the compact radius of the CSRBFs.

The homogeneous solution u_H^{n+1} can be approximated by a linear combination of fundamental solutions (MFS), as follows:

$$u_\mathrm{H}^{n+1} = \sum_{j=1}^{n_\mathrm{s}} \alpha_j^{n+1} G\left(\left\|\mathbf{x} - \boldsymbol{\xi}_j\right\|\right), \tag{1.28}$$

where n_s is the number of the source points $\{\boldsymbol{\xi}_j\}_{j=\overline{1,n_\mathrm{s}}} \notin \overline{D}$ placed outside the spatial domain $\overline{D}$, $\left\{\alpha_j^{n+1}\right\}_{j=\overline{1,n_\mathrm{s}}}$ are unknown coefficients to be determined by a collocation procedure, and G is the fundamental solution of the two-dimensional Laplace equation given by

$$G\left(\|\mathbf{x} - \boldsymbol{\xi}\|\right) = -\frac{1}{2\pi} \ln\left(\|\mathbf{x} - \boldsymbol{\xi}\|\right). \tag{1.29}$$

According to the definitions of u_H^{n+1} and u_P^{n+1}, given by (1.28) and (1.24), respectively, equation (1.22) can be written as

$$\nabla^2 u_\mathrm{P}^{n+1} = C_0\left(u_\mathrm{H}^{n+1} + u_\mathrm{P}^{n+1}\right) + C_1 u^n + C_2 u^{n-1} + C_3 u^{n-2} - g(\mathbf{x}, t^{n+1}). \tag{1.30}$$

Let us define $r_{i,j}$ and $\rho_{i,j}$ as $r_{i,j} = \|\mathbf{x}_i - \mathbf{x}_j\|$ and $\rho_{i,j} = \left\|\mathbf{x}_i - \boldsymbol{\xi}_j\right\|$. Then, substituting equations (1.28) and (1.24) into equation (1.30) and collocating at the field points $\{\mathbf{x}_i\}_{i=\overline{1,n_\mathrm{f}}} \in D$, we obtain

$$\sum_{j=1}^{n_\mathrm{f}} \beta_j^{n+1} \left[f\left(r_{i,j}\right) - C_0 F\left(r_{i,j}\right)\right] - \sum_{j=1}^{n_\mathrm{s}} \alpha_j^{n+1} C_0 G\left(\rho_{i,j}\right) = S(\mathbf{x}_i, t^{n+1}), \quad i = \overline{1, n_\mathrm{f}}, \tag{1.31}$$

where

$$S(\mathbf{x}_i, t^{n+1}) = C_1 u^n(\mathbf{x}_i) + C_2 u^{n-1}(\mathbf{x}_i) + C_3 u^{n-2}(\mathbf{x}_i) - g(\mathbf{x}_i, t^{n+1}). \tag{1.32}$$

Substituting equations (1.28) and (1.24) into the Dirichlet boundary condition in (1.5) and collocating at the boundary points $\{\mathbf{x}_i\}_{i=\overline{n_\mathrm{f}+1, n_\mathrm{f}+n_\mathrm{b}}} \in \partial D$, where n_b is the number of the boundary points satisfying $n_\mathrm{b} \ge n_\mathrm{s}$, we obtain

$$\sum_{j=1}^{n_\mathrm{f}} \beta_j^{n+1} F\left(r_{i,j}\right) + \sum_{j=1}^{n_\mathrm{s}} \alpha_j^{n+1} G\left(\rho_{i,j}\right) = \nu(\mathbf{x}_i, t^{n+1}), \quad i = \overline{n_\mathrm{f}+1, n_\mathrm{f}+n_\mathrm{b}}. \tag{1.33}$$

The equations (1.31) and (1.33) yield the following linear system of algebraic equations:

$$\begin{bmatrix} A_1 & A_2 \\ A_3 & A_4 \end{bmatrix} \begin{bmatrix} \boldsymbol{\beta}^{n+1} \\ \boldsymbol{\alpha}^{n+1} \end{bmatrix} = \begin{bmatrix} \boldsymbol{S} \\ \boldsymbol{\nu} \end{bmatrix}, \tag{1.34}$$

where

$$\begin{aligned}
&\boldsymbol{\beta}^{n+1} = \left[\beta_1^{n+1}, \beta_2^{n+1}, \ldots, \beta_{n_\mathrm{f}}^{n+1}\right]^{\mathrm{T}}, \qquad \boldsymbol{\alpha}^{n+1} = \left[\alpha_1^{n+1}, \alpha_2^{n+1}, \ldots, \alpha_{n_\mathrm{s}}^{n+1}\right]^{\mathrm{T}}, \\
&\boldsymbol{S} = \left[S(\mathbf{x}_1, t^{n+1}), S(\mathbf{x}_2, t^{n+1}), \ldots, S(\mathbf{x}_{n_\mathrm{f}}, t^{n+1})\right]^{\mathrm{T}}, \\
&\boldsymbol{\nu} = \left[\nu(\mathbf{x}_{n_\mathrm{f}+1}, t^{n+1}), \nu(\mathbf{x}_{n_\mathrm{f}+2}, t^{n+1}), \ldots, \nu(\mathbf{x}_{n_\mathrm{f}+n_\mathrm{b}}, t^{n+1})\right]^{\mathrm{T}}, \\
&A_1 \text{ consists of the elements } f\left(r_{i,j}\right) - C_0 F\left(r_{i,j}\right), \quad i = \overline{1, n_\mathrm{f}},\ j = \overline{1, n_\mathrm{f}}, \\
&A_2 \text{ consists of the elements } -C_0 G\left(\rho_{i,j}\right), \quad i = \overline{1, n_\mathrm{f}},\ j = \overline{1, n_\mathrm{s}}, \\
&A_3 \text{ consists of the elements } F\left(r_{n_\mathrm{f}+i,j}\right), \quad i = \overline{1, n_\mathrm{b}},\ j = \overline{1, n_\mathrm{f}}, \\
&\text{and} \\
&A_4 \text{ consists of the elements } G\left(\rho_{n_\mathrm{f}+i,j}\right), \quad i = \overline{1, n_\mathrm{b}},\ j = \overline{1, n_\mathrm{s}}.
\end{aligned}$$

To set up the time marching, the Euler scheme is used to obtain the sub-components u^{-1} and u^{-2} from the initial conditions in (1.5) as follows:

$$u^{-1} = \phi - h\psi, \quad u^{-2} = \phi - 2h\psi. \tag{1.35}$$

After determining the coefficients $\left\{\beta_j^{n+1}\right\}_{j=\overline{1,n_\mathrm{f}}}$ and $\left\{\alpha_j^{n+1}\right\}_{j=\overline{1,n_\mathrm{s}}}$ by solving the linear system of algebraic equations (1.34), the solution u^{n+1} at any point $\mathbf{x} \in \overline{D}$ is obtained explicitly as

$$u^{n+1}(\mathbf{x}) = \sum_{j=1}^{n_\mathrm{f}} \beta_j^{n+1} F\left(\|\mathbf{x} - \mathbf{x}_j\|\right) + \sum_{j=1}^{n_\mathrm{s}} \alpha_j^{n+1} G\left(\left\|\mathbf{x} - \boldsymbol{\xi}_j\right\|\right), \quad \mathbf{x} \in \overline{D}. \tag{1.36}$$

In the next section, the numerical methods described above are applied for the solution of a physical example concerning the determination of the temperature distribution in a biological tissue undergoing laser irradiation.

1.5 Numerical results and discussion

In this physical example, we consider the model (1.1)–(1.3) describing the heat propagation in a rectangular biological skin tissue $\Omega = (0, \bar{L}_1) \times (0, \bar{L}_2)$ with the input data [5, 6, 10]

$$\begin{aligned}
\kappa = 0.5016 \text{ W/(m °C)},\ \rho_\mathrm{t} = 1000 \text{ kg/m}^3,\ c_\mathrm{t} = 4180 \text{ J/(kg °C)}, \\
\rho_b w_b = 8 \text{ kg/(m}^3\text{s)},\ c_b = 3344 \text{ J/(kg °C)},\ \tau = 20 \text{ s},\ T_b = T_0 = \mu = 37°\text{C}, \\
\bar{L}_1 = 0.05\text{m},\ \bar{L}_2 = 0.025\text{m},\ V_0 = Q_m = 0,\ t_\mathrm{f} = 60 \text{ s}.
\end{aligned}$$

The biological skin tissue is assumed to undergo laser irradiation of the form [5]

$$Q_e(\bar{x}_1, \bar{x}_2) = \rho_\mathrm{t} K \Lambda_0 \exp\left(a(\bar{x}_1 - 0.01)\right) \exp\left(\frac{b\bar{x}_2^2}{\bar{x}_1 + c}\right), \quad (\bar{x}_1, \bar{x}_2) \in \left[0, \bar{L}_1\right] \times \left[0, \bar{L}_2\right],$$

where $K = 12.5 \text{ kg}^{-1}, a = -127 \text{ m}^{-1}, b = -129 \text{ m}^{-1}$ and $c = 0.0245$ m are antenna constants, and $\Lambda_0 = 20$ W is the transmitted power.

The above dimensional quantities transform, via (1.4) and (1.6), into the following dimensionless data used as input for the problem (1.5):

$$a_1 = 3.384,\ a_2 = 1.152,\ \phi = \psi = \nu = 0,\ L_1 = 10.7583,\ L_2 = 5.3791,$$
$$g(x_1, x_2, t) = 0.291 \exp\left(-0.5902 x_1 + 1.27\right) \exp\left(\frac{-0.5995 x_2^2}{x_1 + 5.2716}\right).$$

The heat propagation in the single-layer, two-dimensional biological skin tissue is numerically simulated by solving the dimensionless model (1.5) using the ADI scheme and the TMMFS described in Sections 1.3 and 1.4, respectively. We take a mesh size of $M^{(1)} = M^{(2)} = N = 40$ when applying the ADI scheme. In implementing the TMMFS, we take $\lambda = 3$ and consider $n_{\rm f} = 81$ field points, $n_{\rm b} = 84$ boundary points and $n_{\rm s} = 84$ source points uniformly distributed in the spatial domain as shown in Figure 1.1. We take the time interval $h = 0.025$ which is equal to time step used when employing the ADI scheme. For a clearer presentation, we report

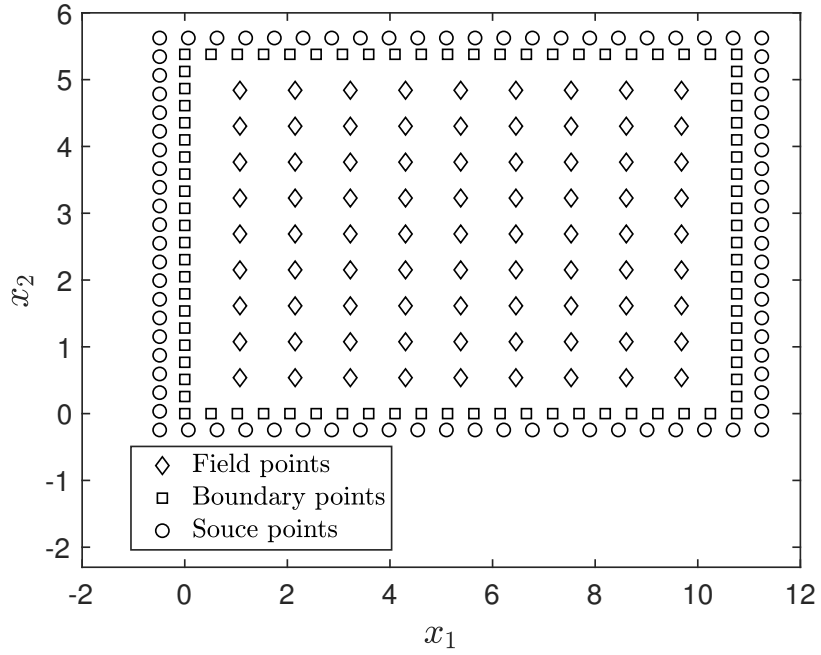

Figure 1.1: Distributions of the field, boundary and source points in the coupled MPS-MFS.

results using the scaled non-dimensional coordinates $\tilde{x}_1 = \bar{x}_1/\bar{L}_1$ and $\tilde{x}_2 = \bar{x}_2/\bar{L}_2$.

Figure 1.2 depicts the numerical solutions obtained by the two methods at various field points, as functions of time t. From this figure, it can be seen that excellent agreement has been achieved. To further confirm the convergence of the numerical solutions, Table 1.1 presents the numerical solutions at various points scattered throughout the space-time domain, and the same conclusion can be observed.

1.6 Conclusions

The physical problem of determining the temperature distribution in a single-layer, two-dimensional biological skin tissue undergoing thermal therapy through laser irradiation has been considered. The thermal-wave model of bio-heat transfer has been used to describe the heat propagation in

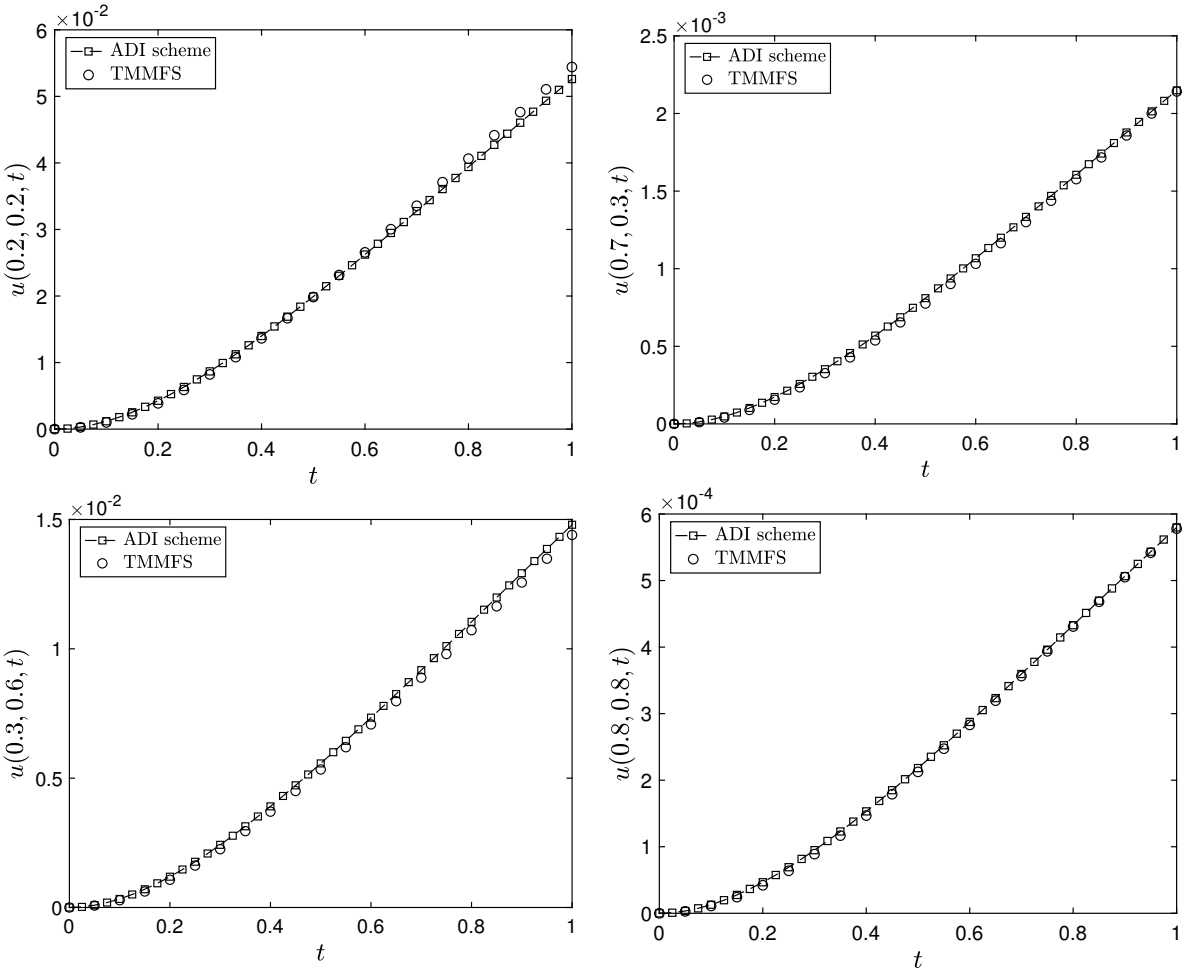

Figure 1.2: The numerical temperature $u(\tilde{x}_1, \tilde{x}_2, t)$ at $(0.2, 0.2, t)$, $(0.7, 0.3, t)$, $(0.3, 0.6, t)$ and $(0.8, 0.8, t)$.

Table 1.1: The numerical solutions at various points in the space-time domain.

$\tilde{x}_1$	$\tilde{x}_2$	t	u_{ADI}	u_{TMMFS}	T_{ADI} (°C)	T_{TMMFS} (°C)
0.1	0.4	0.4	1.8729E–2	1.7393E–2	37.6930	37.6435
0.2	0.3	0.8	3.5082E–2	3.5136E–2	38.2980	38.3000
0.3	0.5	0.2	1.4898E–3	1.3387E–3	37.0551	37.0495
0.4	0.7	0.1	1.5015E–4	1.2760E–4	37.0056	37.0047
0.6	0.6	0.9	2.3539E–3	2.3270E–3	37.0871	37.0861
0.8	0.3	0.5	4.3344E–4	4.1294E–4	37.0160	37.0153
0.9	0.7	0.7	2.3999E–4	2.2985E–4	37.0089	37.0085

such a tissue and numerically solved by an easy-to-implement meshless method. The numerical solution has been validated by a comparison with the results obtained by the ADI scheme, and excellent agreement has been achieved. One can observe that the mesh-free nature of the time-marching method of fundamental solutions (TMMFS) makes it more efficient than mesh-dependent methods. Another feature of the used meshless method is its applicability to

irregular domains. The numerical results obtained can be further tested by a comparison with experimental data. However, this extension is deferred to further work.

Acknowledgements

D. Lesnic would like to acknowledge the support of the EPSRC grant EP/W000873/1 on "Transient Tomography for Defect Detection". No data are associated with this article. For the purpose of open access, the authors have applied a Creative Commons Attribution (CC BY) licence to any Author Accepted Manuscript version arising from this submission.

References

[1] Araujo A., Neves C. and Sousa E. An alternating direction implicit method for a second-order hyperbolic diffusion equation with convection. *Applied Mathematics and Computation*, 239: 17–28, 2014.

[2] Chen C.S., Brebbia C.A. and Power H. Dual reciprocity method using compactly supported radial basis functions. *Communications in Numerical Methods in Engineering*, 15(2): 137–150, 1999.

[3] Houbolt J.C. A recurrence matrix solution for the dynamic response of elastic aircraft. *Journal of the Aeronautical Sciences*, 17(9): 540–550, 1950.

[4] Jalali A., Ayani M.-B. and Baghban M. Simultaneous estimation of controllable parameters in a living tissue during thermal therapy. *Journal of Thermal Biology*, 45: 37–42, 2014.

[5] Kouremenos D.A. and Antonopoulos K.A. Heat transfer in tissues radiated by a 432 MHz directional antenna. *International Journal of Heat and Mass Transfer*, 31(10): 2005-2012, 1988.

[6] Kumar D. and Rai K.N. Numerical simulation of time fractional dual-phase-lag model of heat transfer within skin tissue during thermal therapy. *Journal of Thermal Biology*, 67: 49–58, 2017.

[7] Lin C.Y., Gu M.H. and Young D.L. The time-marching method of fundamental solutions for multi-dimensional telegraph equations, *Computers, Materials & Continua*, 18(1): 43–68, 2010.

[8] Liu J., Chen X. and Xu L.X. New thermal wave aspects on burn evaluation of skin subjected to instantaneous heating. *IEEE Transactions on Biomedical Engineering*, 46(4): 420–428, 1999.

[9] Mitra K., Kumar A., Vedevarz A. and Moallemi M. Experimental evidence of hyperbolic heat conduction in processed meat. *Journal of Heat Transfer*, 117: 568–573, 1995.

[10] Ozen S., Helhel S. and Cerezci O. Heat analysis of biological tissue exposed to microwave by using thermal wave model of bio-heat transfer (TWMBT). *Burns*, 34(1): 45–49, 2008.

[11] Qin J. The new alternating direction implicit difference methods for the wave equations. *Journal of Computational and Applied Mathematics*, 230(1): 213–223, 2009.

[12] Ren Z.P., Liu J., Wang C.C. and Jiang P.X. Boundary element method (BEM) for solving normal or inverse bio-heat transfer problem of biological bodies with complex shape. *Journal of Thermal Science*, 4: 117–124, 1995.

[13] Wainwright P. Thermal effects of radiation from cellular telephones. *Physics in Medicine & Biology*, 45: Art. 2363, 2000.